High-Performance Thin-Film Lithium Niobate Mach-Zehnder Modulator on 8-Inch Silicon Substrate

Jingjie Zhou[(1)], Qingyu Cong[(1)], Liming Lv[(2)], Zhanshi Yao [(3)], Shiyang Zhu [(3)], Yuxi Wang [(3)], Zhaoyi Li[(1)], Zuowen Fan[(1)], Xianfeng Zeng[(4)], Ting Hu[(1)] , Lianxi Jia [(1,2,4),*]

(1) School of Microelectronics, Shanghai University, Shanghai, P. R. China
(2) Shanghai Industrial μTechnology Research Institute, Shanghai, P. R. China
(3) Huawei Technologies, B&P Lab, Shenzhen, P. R. China
*(4) Shanghai Institute of Microsystem and Information Technology, Chinese Academy of Sciences, Shanghai, P. R. China, *jialx@mail.sim.ac.cn*

Abstract: We first report the thin-film lithium niobate (TFLN) electro-optic Mach-Zehnder modulator (MZM) on an 8-inch silicon substrate fabricated in the back-end-of-line (BEOL) of CMOS foundry. It operates at 1550 nm with electro-optical response of only 1.5 dB roll-off at 67 GHz. © 2024 The Author(s)

1. Introduction

Due to the high optical confinement, superior electro-optical (EO) bandwidth, and minimal optical losses [1,2], the TFLN modulator plays an important role in high-speed optical communication and interconnect [3]. Recently, further improvement in modulation performance by utilizing T-shaped electrodes and either quartz substrate [4] or hollowed-out silicon substrate [5] is reported. However, it is still challenging for the large-scale production of TFLN modulators [6] limited by the wafer size and capability of fabrication tools.

In the past, TFLN modulators were demonstrated with chips or 4- and 6-inch wafers [7,8]. Two methods were used to form the waveguide. One is to etch the LN directly to form channel or slab waveguides. The other method involves the direct bonding of unetched TFLN with patterned Si/SiN waveguides, utilizing the integration and scalability of LN's Pockels effect with silicon photonics [9,10]. However, this method suffers from limitations in light confinement and additional coupling losses between LN and Si/SiN waveguides.

In this work, we design and fabricate an LNOI electro-optic modulator on an 8-inch Si substrate. The propagation loss of the LN ridge waveguide at 1550 nm is 0.47 dB/cm. The measured EO response exhibits only 1.5 dB roll-off at 67 GHz, with a $V\pi \cdot L$ of 3.12 V·cm. Finally, we perform the modulation experiments with four-level pulse amplitude modulation (PAM-4) signals and record open eye diagram up to 120 Gbps.

2. Device Fabrication

The device was fabricated in a commercial 8-inch foundry with a 6-on-8-inch LNOI wafer (commercially available from NANOLN). The fabrication process developed in this work can be directly applied to full 8-inch LNOI wafers once they become available in future. As shown in Figs. 1(a-h), the LNOI wafer consists of a 600-nm thick 6-inch X-cut TFLN, a 3-μm thick buried oxide (BOX) layer, and an 8-inch Si substrate. The I-line lithography is employed to pattern the waveguide. To achieve a steeper sidewall angle, a SiO2 layer deposited by PECVD is used instead of photoresist (PR) as hard mask for the etching of LN. The etching depth of LN is 300 nm. A SiO2 cladding layer is then deposited with PECVD as both cladding and isolation to the metal electrode. The aluminum electrode with thickness of 1 μm is fabricated for electrical signals transmission.

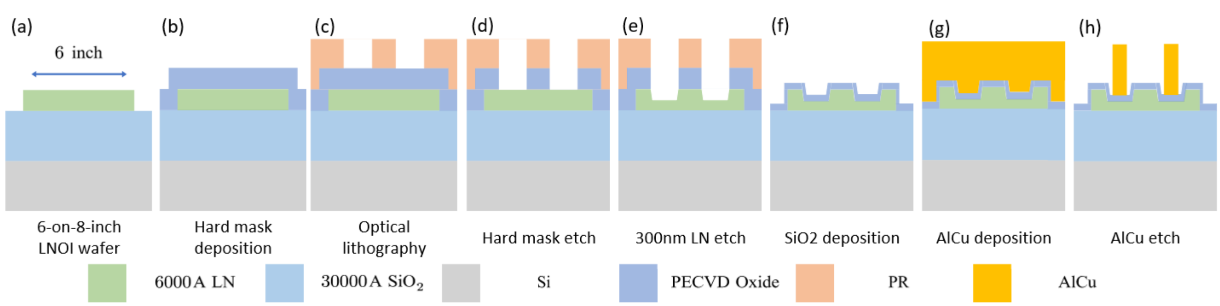

Fig. 1: Key fabrication steps of TFLN electro-optic modulators: (a) Starting with 6-on-8-inch LNOI wafers, (b) Deposition of SiO2 using PECVD, (c) Waveguide patterning using i-line optical lithography, (d) Dry etching of SiO2 hard mask, (e) Partial dry etching of LN. (f) SiO2 cladding using PECVD. (g) Sputtering of Al metal film. (h) Etching and cleaning of Al electrode.

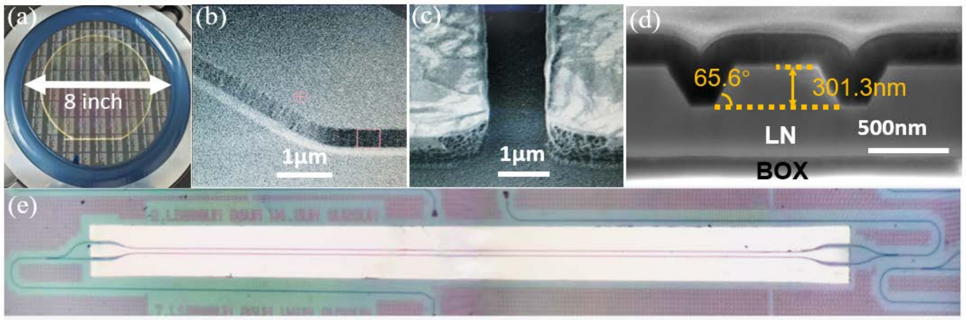

Fig.2: (a) Photography of the fabricated LNOI wafer. (b) The SEM image of the etched LN waveguide. (c) The SEM image of the metal slit in the narrow gap. (d) Cross-sectional view of the grating produced by FIB. (e) Photography of the LNOI modulator.

A photography of the fabricated wafer with a clear edge of the 6-inch LN on an 8-inch Si substrate is shown in Fig. 2(a). The scanning electron microscope (SEM) images of LN waveguides and the aluminum electrode in the narrow gap are shown in Figs. 2(b) and 2(c), respectively. A further inspection of the LN waveguide using focused ion beam (FIB) is shown in Fig. 2(d), which indicates that the smooth sidewalls of the waveguides are achieved. In comparison to the results in the reference [11], a much deeper etching depth is achieved while the sidewall profile keeps the same quality. The fabricated LNOI modulator is shown in Fig. 2(e).

3. Device Design and Characterization

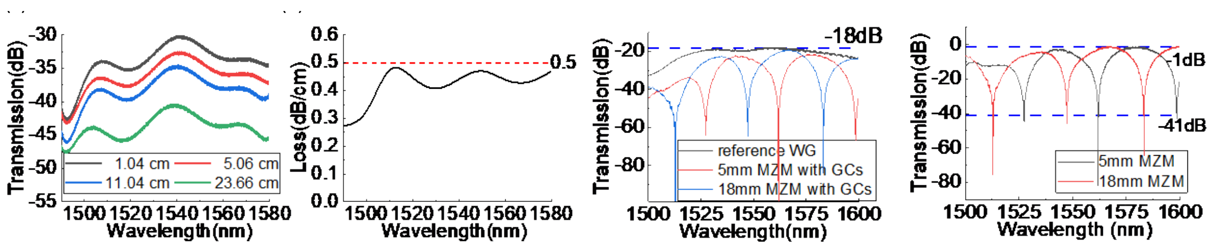

Fig.3: (a) The optical insertion loss of waveguides with width of 1 μm and lengths of 1.04 cm, 5.06 cm, 11.04 cm, and 23.66 cm. (b) The calculated propagation losses at different wavelength. (c) The measured insertion loss of reference waveguide, 5mm MZM, and 18mm MZM. (d) The normlized insertion loss of the 5mm and 18mm MZM.

The measured insertion loss of LN ridge waveguides in the cutback structure and the calculated propagation loss at different wavelengths are shown in Figs. 3(a) and 3(b), respectively. A propagation loss smaller than 0.5dB/cm in the whole spectrum proves the high quality of the fabricated LN waveguide. The measured insertion loss of the reference waveguide with negligible length and MZMs with modulation lengths of 5 mm and 18 mm are shown in Fig. 3(c). The normalized insertion loss of the 5mm and 18mm MZM with the reference waveguide are shown in Fig. 3(d). An extinction ratio exceeding 40 dB is demonstrated, indicating an excellent performance of the multimode interferometers (MMIs). By comparing the two peak values around 1550 nm of the two MZMs, the calculated propagation loss of the modulation waveguide is 0.38 dB/cm, which is consistent to the measured slab waveguide shown in Fig. 3(b), conveying that the electrode does not introduce extra absorption loss. In addition, the extracted insertion loss of each MMI is around 0.3 dB.

In the phase shift part of the MZM, a waveguide with width of 4.5 μm is used to reduce the propagation loss and improve the modulation efficiency. The cross-section of the designed MZM is shown in Fig. 4 (b). The CPW electrode with gap of 6 μm. Modulation efficiency can be improved by simultaneously reducing the electrode spacing and waveguide width. In this work a large electrode spacing is set in order to avoid the absorption of light by the electrodes. Fig.4(c) shows the test results of modulation efficiency with similar method in reference [12]. There is an offset between two signals due to different delay of the two connection, but it can still get a V_π of 6.24V. Fig. 4(d) shows the EE S parameters of the CPW electrodes measured using a vector network analyzer (VNA) with a bandwidth of 67 GHz, based on which the microwave phase index nm is extracted to be 2.4 and the characteristic impedance Z0 to be 47 Ω, as shown in Fig. 4(e). The propagation loss of the CPW electrode is shown in Fig. 4(f), which is relatively higher than that of Au CPW electrode [4]. The loss of the CPW electrode can be reduced by increasing the thickness of the Al electrode and removing the underlying silicon substrate through etching [5,13,14], which will be considered in our future work. The frequency response normalized to the response at 1 GHz is shown in Fig. 4(g), indicating that the bandwidth exceeds 67 GHz with only 1.5 dB roll-off. The data rate up to 120 Gbps with PAM-4 signal is demonstrated in Fig. 4(h). In the measurement, no pre-emphasis or line coding are used to compensate the potential spectral attenuation in the detector or other components.

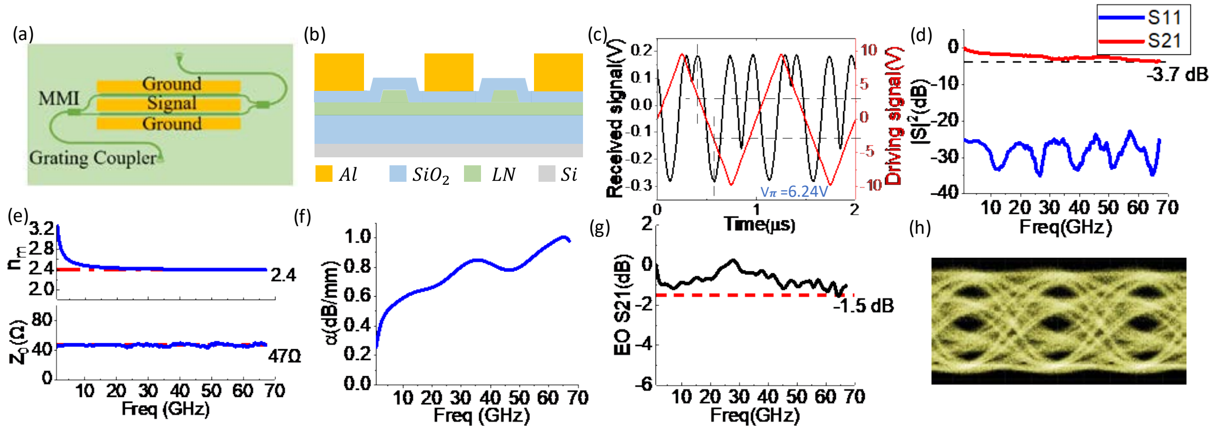

Fig. 4: (a) Schematic of a MZM. (b) Cross-section of the electro-optic modulation region of the MZM. (c) The measured electrical-optical response and the driving signal at 1MHz. (d) The measured electrical-to-electrical (EE) S-parameters. (e-f) The extracted group index, impedance, and propagation loss of the electrode. (g) Measurement result of the EO bandwidth. (h) The measured eye diagram of 60 Gbaud PAM-4 signal.

4. Conclusion

In conclusion, we first report the demonstration of TFLN modulator on an 8-inch wafer, showcasing the feasibility of using the BEOL process to fabricate TFLN devices in an 8-inch fab. We demonstrate the high performance TFLN modulator with only 1.5 dB roll-off at 67 GHz with a $V\pi \cdot L$ value of 3.12 V·cm. This work establishes the foundation for large-scale manufacturing of TFLN photonic integrated circuits with commercial 8-inch CMOS line.

5. Acknowledgements

This work was supported by National Key Research and Development Program of China (2018YFB2200500). We also acknowledge the assistance provided by SJTU-Pinghu Institute of Intelligent Optoelectronics in the testing process.

6. References

[1] C. Wang et al., "Integrated lithium niobate electro-optic modulators operating at CMOS-compatible voltages," Nature 562, 101–104 (2018).
[2] D. Zhu et al., "Integrated photonics on thin-film lithium niobate," Advances in Optics and Photonics 13, 242-352 (2021).
[3] M. Xu et al., Thin-Film Lithium Niobate DP-IQ Modulator for Driverless 130 Gbaud 64 QAM Transmission," in Optical Fiber Communication Conference (2022), pp. Th1J.2.
[4] P. Kharel et al., "Breaking voltage–bandwidth limits in integrated lithium niobate modulators using micro-structured electrodes," Optica 8, 357-363 (2021).
[5] Y. Xue et al., "Breaking the bandwidth limit of a high-quality-factor ring modulator based on thin-film lithium niobate," Optica 9, 1131-1137 (2022).
[6] J. Wang et al., "Toward photonic–electronic convergence based on heterogeneous platform of merging lithium niobate into silicon," Journal of the Optical Society of America B 40, 1573-1590 (2023).
[7] K. Luke et al., "Wafer-scale low-loss lithium niobate photonic integrated circuits," Optics Express, 28, 24452-24458 (2020).
[8] J. Leo et al., "Wafer-scale fabrication of low-loss waveguides in lithium niobate on insulator (LNOI) integrated photonics platform," in European Conference on Optical Communication (2022), pp. Mo3F.4.
[9] M. He et al., "High-performance hybrid silicon and lithium niobate Mach–Zehnder modulators for 100 Gbit s−1 and beyond," Nature Photonics 13, 359–364 (2019).
[10] A. N. R. Ahmed et al., "High-efficiency lithium niobate modulator for K band operation," APL Photonics 5, 091302 (2020).
[11] H. Wang et al., "Thin-film Lithium Niobate Photonic Devices on 8-inch Silicon Substrates," in Optical Fiber Communication Conference (2023), pp. W2B.1.
[12] F. Yang et al., "Monolithic thin film lithium niobate electro-optic modulator with over 110 GHz bandwidth," Chinese Optics Letters 20, 022502 (2022).
[13] G. Ghione, "Semiconductor Devices for High-Speed Optoelectronics," Cambridge: Cambridge University Press (2009).
[14] P. O. Weigel et al., "Bonded thin film lithium niobate modulator on a silicon photonics platform exceeding 100 GHz 3-dB electrical modulation bandwidth," Optics Express 26, 23728-23739 (2018).